JOURNAL OF CATALYSIS 93, 135–151 (1985)

Catalytic Hydrodemetallation of Nickel Porphyrins

III. Acid–Base Modification of Selectivity

ROBERT A. WARE[1] AND JAMES WEI[2]

Department of Chemical Engineering, Massachusetts Institute of Technology, Cambridge, Massachusetts 02139

Received March 29, 1984; revised November 27, 1984

The reaction network of metallo-porphyrins characteristic of metal-bearing species in residuum oil proceeds through a consecutive pathway during catalytic hydrodemetallation, involving hydrogenation prior to the final ring opening and metal-deposition step. The intrinsic reaction selectivity over commercial $CoO–MoO_3/Al_2O_3$ catalyst, defined as the ratio of hydrogenation rate/metal-deposition rate of Ni-tetra(3-methylphenyl) porphyrin dissolved in a clean mineral oil and reacted at 345°C and 6.99 MPa H_2, was varied with acid–base additives of different electronic character. A dramatic shift in the overall rate-limiting step from hydrogenation to ring opening in the demetallation sequence was observed. Alkali dopants (Cs, Na) significantly reduced catalyst acidity and the metal-deposition activity, with only a marginal reduction in hydrogenation activity. Treatment with halogens (I, Cl) in a reducing environment enhanced the metal-deposition activity but suppressed the hydrogenation activity of the catalyst. Sulfiding had the unique effect of producing an enhancement in both the hydrogenation and metal-deposition activities relative to the oxide catalyst. The impact of these selective reaction changes was manifested in the metal-deposition profiles generated under diffusion-limited conditions.

I. INTRODUCTION

Demetallation reactions occurring under strongly diffusion-limited conditions would lead to rapid catalyst deactivation from a concentration of deposited metals at the catalyst periphery, excluding access to the inner unpoisoned regions of the catalyst. Shape and size variations and incorporation of larger pores into the catalyst have demonstrated the potential for increasing the metal capacity of a catalyst (*1–3*).

An alternative approach is to control the selectivity of the hydrodemetallation reactions in order to control the location of metal deposition within catalyst pellets. The demetallation network of nickel porphyrins has been demonstrated in Parts I (*4*) and II (*5*) of this series to consist of hydrogenation and hydrogenolysis. This implies a dual functionality to the hydrotreating catalyst. Similar dual-function interpretations have been used in the discussions of hydrodesulfurization (HDS) and hydrodenitrogenation (HDN) reaction networks (*6, 7*). Through judicious modification of the catalyst surface one type of reaction may be enhanced or inhibited with respect to the other, thus altering the selectivity of the overall metal removal reaction. Ability to direct the metal deposition to specific sites in a catalyst would potentially avoid problems of pore-mouth plugging. Alternatively, if complete separation of the two types of reactions were achieved, poisoning of CoMo catalysts could be avoided in a two-stage operation.

Numerous attempts and methods for altering the catalytic properties of $Co(Ni)Mo/Al_2O_3$ hydrotreating catalysts have been reported. These generally have been motivated by the desire to control one func-

[1] Present address: Mobil Research and Development Corp., Paulsboro, N.J. 08066.

[2] To whom correspondence should be addressed.

0021-9517/85 $3.00

tion of the catalyst to improve activity and selectivity for HDS and HDN. These reactions, while similar to hydrodemetallation (HDM), are different in one important aspect. They are not inherently deactivating. The heteroatom is removed as a gaseous product (H_2S, NH_3) rather than deposited as a permanent poison on the catalyst surface.

In this investigation a series of modified catalysts was prepared to examine the influence of surface treatment with dopants of varying electronic character on the HDM reaction network of Ni-tetra(3-methylphenyl)porphyrin (Ni-T3MPP). The additives included Cs, Na, S, I, and Cl with the oxide $CoMo/Al_2O_3$ catalyst (HDS-16A) as the base or reference catalyst. The catalysts were prepared by modifying the existing commercial catalyst rather than the alumina support prior to Co and Mo impregnation.

The method of addition may alter the influence that the additive exerts in controlling surface properties of the catalyst, but there is controversy in the literature as to whether this difference is always detectable in catalytic activity measurements. Massoth and co-workers (*8*), in a systematic study on the effects of dopants of varying acidity on the desulfurization, hydrogenation, and cracking activity of modified $CoMo/Al_2O_3$ catalysts, observed no difference based on the order of addition. Basic additives such as Na and Ca at low loadings (0.5 wt%) resulted in a lowering of both HDS and cracking activity. Similarly, the addition of F and Cl increased the HDS and cracking rates. Hydrogenation activity was the function least affected by the additives. Boorman *et al.* (*9*) observed similar patterns of behavior but, unlike Massoth, the magnitude of the change was dependent on the order of addition of the Na and F dopants.

The presence of additives such as Na (*10, 11*), P (*12, 13*), and F (*9*) on the support is known to affect the surface acidity, the support/metal interaction, and the coordination of Co and Mo after impregnation. An extensive investigation probing the surface structure and properties of Co–Mo catalysts supported on γ-Al_2O_3 and doped with alkali metals (Li, Na, K, Rb, and Cs) has been conducted by Lycourghiotis and co-workers (*14–16*). Activity variations in the relatively facile HDS of thiophene were observed indicating substantial modification of surface characteristics (*17, 18*).

In contrast, the addition of dopants to the calcined catalyst is not expected to significantly influence the structural characteristics of the Co and Mo phases already present on the catalyst. Coordination of dopant with sites on these metals is likely, however, in addition to dopant interaction with the support, potentially modifying the activity of these metals. Similarly, modification of the total surface acidity can be achieved by adding dopants of various acid character. A decrease in surface acidity has been reported by Martinez and Mitchell (*19*) upon addition of the basic component Mg to a $CoMo/Al_2O_3$ catalyst.

This paper deals with the application of catalyst doping as a technique to modify the relative reaction rates in the demetallation sequence of a model nickel porphyrin. This approach may potentially provide control of metal-deposition location during resid upgrading.

2. EXPERIMENTAL METHODS

A model oil system analogous to that described in Part I (*4*) was again used in this investigation. Ni-tetra(3-methylphenyl) porphyrin (Midcentury Chemicals, Posen, Ill.) dissolved in a white mineral oil (Nujol) at 65 ppm Ni (by weight) comprised the model oil. The mineral oil itself was free of sulfur, nitrogen, and metal compounds and was essentially inert under reaction conditions.

The catalysts were prepared by modifying a commercial $CoO–MoO_3/\gamma$-Al_2O_3 hydrodesulfurization catalyst (American Cyanamid HDS-16A) with dopants of different

electronic character. The reference or base-case catalyst was the CoMo catalyst in the oxide form. All results reported were obtained on 170–200 mesh (74–88 μm diameter) particles which had been shown to yield true intrinsic data, that is, free of diffusional limitations.

The cesium- and sodium-doped samples were prepared by the incipient wetness technique. $CsNO_3$ (Aldrich Chemical) and $NaNO_3$ (J. T. Baker Chemical) were prepared in distilled water to give solutions that upon impregnation would result in nominal alkali cation concentrations of 2.0 mmole/g fresh HDS-16A. This level was chosen to exceed the concentration required to neutralize all the acid sites on the alumina (*14*). The final catalysts were calcined in air at 550°C for 8 hr.

The sulfided catalyst was prepared using a standard procedure recommended by American Cyanamid reported in Part II (*5*). During a demetallation run 0.05 wt% CS_2 (Mallinckrodt) was intentionally added to the feed to stabilize activity by maintaining the catalyst in the sulfided form (*20*).

The iodized and chlorided catalysts were prepared by similar procedures under reducing conditions. Hydrogen, saturated with CH_3I (J. T. Baker Chemical) or $CHCl_3$ (Anachemia) by bubbling through a vessel containing the appropriate liquid at 40 psig and 25°C, was passed over the catalyst at GHSV = 1000 hr^{-1} and 345°C for 3 to 4 hr. The formation of HI and CH_4 from CH_3I and, similarly, HCl and CH_4 from $CHCl_3$ is strongly favored thermodynamically under the conditions used. No source of iodine or chlorine was in the feed oil during the demetallation runs on the prehalided catalysts. This method of addition was different from the more common approach of adding halogens in the form of their ammonium salts via an impregnation step (*8, 9*).

A second procedure was also demonstrated to be effective for chloriding the fresh oxide catalyst. This involved chloriding *in situ* (i.e., during the demetallation reactions) with $CHCl_3$ in the feed in a Cl/Ni atomic ratio of 10. Stable chlorided catalyst activity was achieved after 100 hr on stream.

All of the above-discussed doping procedures were determined to be reliable for obtaining catalysts with no internal gradients. Analysis by scanning electron microscope (SEM) (AMR Model 1000A) equipped with an energy dispersive X-ray analyzer (Tracor Northern Model TN 2000) revealed uniform dopant concentration (to within the 1-μm resolution of the instrument) in all samples.

Modified catalysts were analyzed by Galbraith Laboratories (Knoxville, Tenn.) for dopant concentrations. These results are summarized in Table 1. The concentration of dopant varied substantially from sample to sample when considered on a weight basis. In contrast, when these concentrations were calculated on a comparable basis, i.e., millimole dopant/gram fresh CoMo catalyst, the additive levels were essentially equivalent. Similarly, BET surface areas of the doped samples were approximately the same when calculated on the basis of weight of fresh CoMo oxide catalyst.

There was no attempt to investigate the dependence of catalytic activity on the level of dopant concentration or to determine the minimum requirement for an effect. The molar concentration of each additive on the catalyst was greater than the molar concentration of the Co and Mo metals (0.8 mmole/g cat.). This ensured that their influence would not be overshadowed by the activity of the base-case oxide catalyst, which would have been the case if the dopant were present in trace quantities.

The sulfur concentration measured may represent a lower limit attainable from the sulfiding treatment used. This sample was exposed to air at room temperature prior to analysis, which may have led to removal of sulfur through oxidation of the top sulfide layers (*21*).

Identification of the chemical nature of the halogens on the catalyst surface was attempted using X-ray photoelectron spec-

TABLE 1

Modified Catalyst Properties

	Dopant concentration		Surface area	
	wt%	mmole/g CoMo cat.	m^2/g	m^2/g CoMo cat.
Co–Mo/γ-Al_2O_3 (HDS-16A)[a]	—	—	176[b]	176
Cs–CoMo/Al_2O_3	22.6	2.20	130	168
Na–CoMo/Al_2O_3	4.30	1.95	175	182
Presulfided CoMo/Al_2O_3	4.83	1.59	170	178
Preiodized CoMo/Al_2O_3	19.0	1.85	145	179
Prechlorided CoMo/Al_2O_3	11.5	3.6 (4.3 mmole/g Al_2O_3)	155	175
In situ chlorided CoMo/Al_2O_3	6.3	1.89	—	—
γ-Al_2O_3	—	—	219	—
Prechlorided γ-Al_2O_3	6.36	1.92 mmole/g Al_2O_3	—	—

[a] Base catalyst 5.7 wt% CoO (0.79 mmole Co/g CoMo catalyst); 12.2 wt% MoO_3 (0.85 mmole Mo/g CoMo catalyst).

[b] Surface area based on alumina is 214 m^2/g Al_2O_3.

troscopy (XPS) with a Physical Electronics Model 548 spectrophotometer. Magnesium $K\alpha$ radiation was used as the excitation source. The samples were not prepared in the instrument environment and came in contact with air prior to analysis. Samples were prepared by pressing catalyst powder into 13-mm-diameter disks and then gold decorated. All spectra were referenced to Au $4f_{7/2}$ at 84.0 eV which was equivalent to C 1*s* at 284.4 eV. The binding energies for Al $2p$ = 74.2 eV, Mo $3d_{5/2}$ = 232.7 eV, Mo $3d_{3/2}$ = 236.1 eV, Co $2p_{3/2}$ = 781.7 eV, and Co $2p_{1/2}$ = 797.3 eV. These core levels measured on the oxide catalyst were similar to values reported by Chin and Hercules (*22*).

The aluminum $2p$ level on the iodized catalyst was unchanged from the oxide catalyst, indicating the alumina support was not chemically modified by iodine. In contrast, the aluminum signal on the chlorided catalyst displayed a shoulder at binding energies higher than the support, suggesting some chloriding of the alumina had occurred.

The results for molybdenum indicated a reduction of Mo(VI) present as MoO_3 on the fresh catalyst (Mo $3d_{5/2}$ = 232.7 eV) to Mo(V) (Mo $3d_{5/2}$ = 232.0 eV) and Mo(IV) (Mo $3d_{5/2}$ = 229.0 eV) oxide species (determined from reference values reported by Zingg *et al.* (*23*)) during chlorine and iodine treatment in the reducing environment. A shoulder at 230.8 eV above the Mo(IV) peak on the chlorided catalyst suggested, albeit not definitely, the presence of a chlorided Mo(IV) species (unsupported $MoCl_4$, Mo $3d_{5/2}$ = 230.5 eV)—reported by Walton (*24*).

Data for Mo binding energies in Mo–I complexes were not found in the literature. The similarities in the electron configurations of chlorine and iodine and in the Mo signal for the two catalyst systems suggested that the presence of Mo–I species on the catalyst was possible.

The Co $2p_{3/2}$ and $2p_{1/2}$ levels on the chlorided and iodized samples were essentially unchanged from the fresh oxide catalyst. Binding energies for chlorided cobalt (unsupported $CoCl_2$, Co $2p_{3/2}$ = 783.5 eV) and iodized cobalt (unsupported CoI_2, Co $2p_{3/2}$ = 782.3 eV) reported by Frost *et al.* (*26*) were absent. This may have resulted in part from the inaccessibility of cobalt to the chlorine or iodine due to its existence under the molybdenum layer and strong interaction with the alumina (*25*). There was like-

TABLE 2

TPAD Titration Results

	meq sites/g	meq sites/cm^2 × 10^6	T_{max}[a] (°C)	Acidic effluent
Fresh $CoMo/Al_2O_3$	0.549	0.31	180	no
Cs doped	0.014	0.010	—	no
Na doped	0.029	0.016	—	no
Presulfided	0.546	0.32	189	yes
Preiodized	0.658	0.45	180	yes
Prechlorided	0.547	0.35	173	yes
γ-Alumina	0.08	0.037	318[b]	no

[a] Precision ± 5°C.
[b] Precision ± 10°C.

wise no indication of metallic cobalt (Co $2p_{3/2}$ = 778.1 eV) present on the surface reported by Chin and Hercules (*22*). This was not considered surprising as metallic cobalt is oxidized upon exposure to air (*27*).

From the limited XPS results it was postulated that the majority of the Cl and I was associated with Mo on the catalyst. Chlorine also appeared to be associated with Al whereas iodine was not. No evidence for cobalt–halogen bonding was found.

In conjunction with the chemical characterization of the catalysts, temperature-programmed ammonia desorption (TPAD) was performed on the samples using a DuPont thermogravimetric analyzer with a Metrohm titration assembly. Listed in Table 2 are the acid site equivalents and peak desorption temperatures for the catalysts and the alumina support. The peak desorption temperature was essentially the same for the fresh and modified catalysts, suggesting the surfaces are primarily composed of sites of similar strength and that differences in acidity reflect a difference in number of sites. When compared to the fresh catalyst in Fig. 1, the presulfided (and prehalogenated) catalyst showed a steeper descent on the high-temperature side of the ammonia desorption profile indicative of a slightly lower concentration of strong sites. This, however, may be misleading as above 400°C an acidic effluent was detected with the S-, I-, and Cl-treated catalysts. The onset of desorption of acidic species from these catalysts would mask any ammonia desorbing simultaneously. Thus the acid site concentrations reported for these samples likely represent minimum values.

Results presented in this paper were ob-

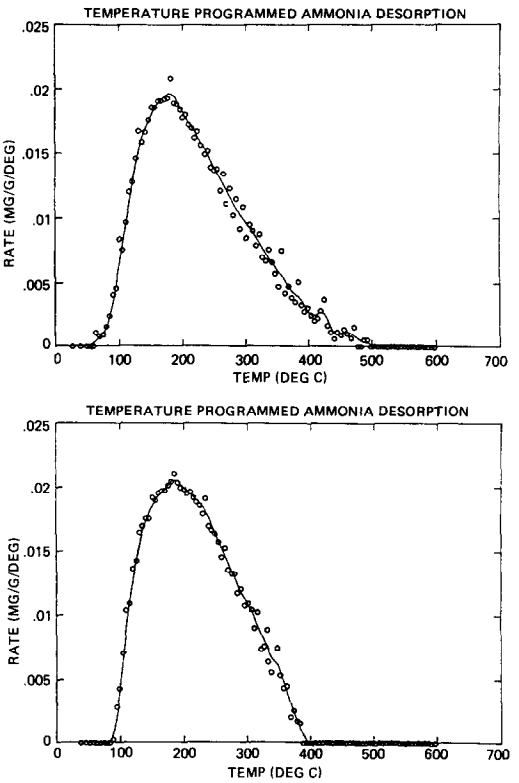

FIG. 1. Ammonia desorption profiles for the oxide (top) and sulfided (bottom) $CoMo/Al_2O_3$ catalysts.

tained under reaction conditions of 345°C and 6.99 MPa H_2 (1000 psig) in a flow microreactor. All measurements were on catalyst batches that had been aged 60 to 100 hr. Analysis of total nickel concentration in the effluent oil was obtained by atomic absorption spectrophotometry. Porphyrinic nickel species were identified by uv–visible spectrophotometry at their wavelengths of characteristic absorbance. Analytical and experimental procedures have previously been discussed (*4, 28*).

3. KINETIC RESULTS ON MODIFIED CATALYSTS

a. Initial Transient Results

All catalyst charges were observed to go through an initial transient period in activity similar to that described previously by Agrawal (*29*) for the oxide catalyst. The initial deactivation, attributed to coke buildup, was not as rapid on the Cs- and Na-doped samples as on the oxide catalyst. This was expected considering the neutralizing influence of these components on the acid sites of the catalyst responsible for cracking and coke deposition.

There was evidence to suggest that the iodine and chlorine on the freshly prepared samples were gradually stripped from the surface in the high-pressure hydrogen environment. Runs conducted on the pretreated catalysts did not have an I or Cl source in the feed so this stripping phenomenon was not surprising. Analysis of the spent iodized catalyst after 200 hr on stream revealed an iodine content of less than 0.1 mmole I/g catalyst. Kinetic measurements were taken during the initial period (50 hr on stream) of relatively stable activity.

Kinetic runs conducted with chlorine ($CHCl_3$) in the feed to induce chloriding of the catalyst (i.e., during reaction with oil) did not experience this long-term deactivation attributed to halogen removal. Analysis of this *in situ* chlorided catalyst after 375 hr on stream revealed a chlorine loading equivalent to 1.89 mmole Cl/g oxide CoMo catalyst (see Table 1). This presumably represents a steady-state chlorine loading on the catalyst. Kinetic data quantitatively similar to those obtained on this catalyst were obtained with the prechlorided catalyst after 75 hr on stream. This suggests that the fresh prechlorided sample was stripped to a chlorine loading similar to that of the *in situ* treated sample or that the catalytic activity was insensitive to the dopant loading at these concentrations.

b. Steady-State Kinetic Results

Concentration profiles (ppm of nickel versus contact time) for Ni-T3MPP reaction at 345°C and 6.99 MPa H_2 are shown in Figs. 3 through 8 for each of the five modified catalysts and the base-case oxide catalyst. The contact times, W/Q, were calculated on the basis of 0.7 g of oxide catalyst charged to the reactor. This was necessary because the weight of catalyst after *in situ* S, I, and Cl treatment was not known. Similarly, when the weight of the modified catalyst was known (Cs- and Na-doped), an amount of catalyst equivalent to 0.7 g oxide Co–Mo catalyst was used.

There are several key points to consider in proceeding through the six figures, the first being the kinetic characteristics revealed by the rate of total metal removal and the relative rate of feed porphyrin (Ni-P) removal to total metal removal. These give an indication as to the influence of the additive on the overall catalytic activity and, more importantly, the impact on the selectivity within the demetallation sequence. Second, the generation of similar nickel intermediates on all catalysts demonstrates that the pathway of Ni-T3MPP demetallation discussed in Part I (*4*) on the oxide CoMo catalyst and shown in Fig. 2 is unchanged in the presence of these additives.

For the alkali metal-doped samples (Figs. 3 and 4), feed porphyrin was rapidly hydrogenated, forming the Ni-PH_2 and Ni-PH_4 species. These three, as evidenced by the constant relative concentration ratios, then maintained a dynamic equilibrium indica-

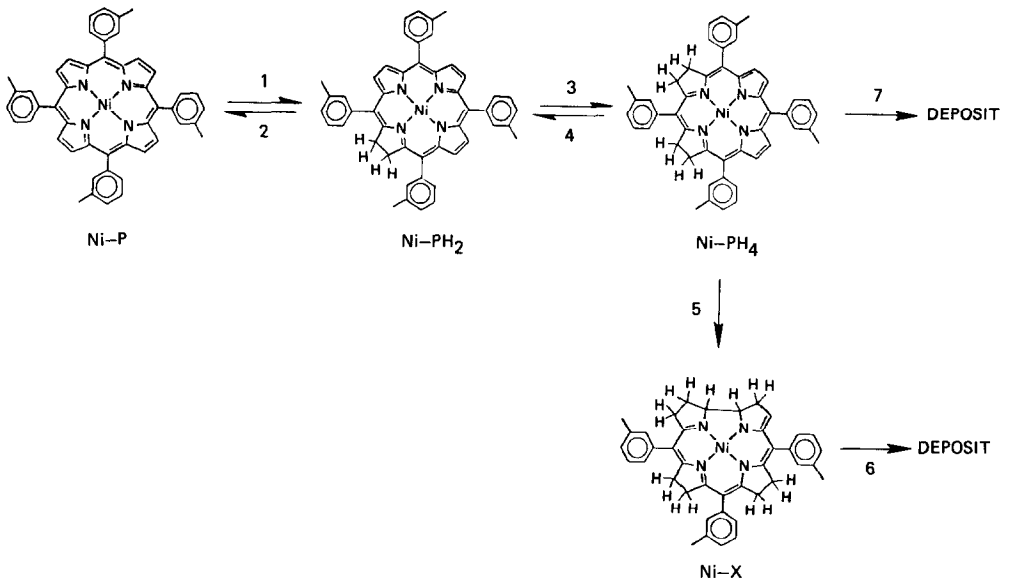

FIG. 2. Reaction pathway for Ni-T3MPP demetallation.

tive of relatively rapid hydrogenation/dehydrogenation reactions. The lack of Ni-*X* present with the cesium-doped catalyst and the low concentration with the sodium sample indicated high ratios of k_7/k_5 which switched Ni-PH_4 to deposition without Ni-

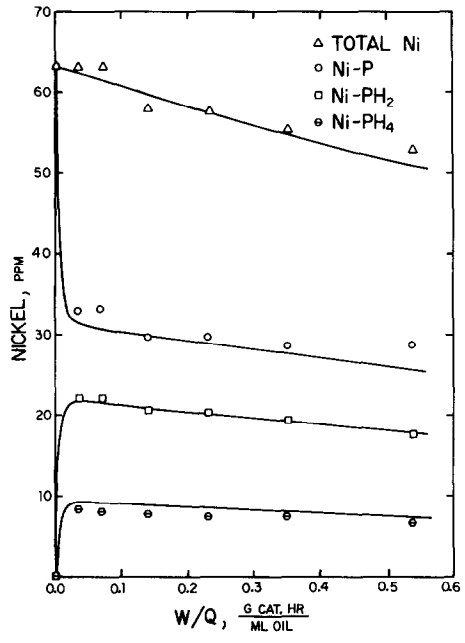

FIG. 3. Concentration versus contact time results for Ni-T3MPP at 63 ppm Ni feed, 345°C, and 6.99 MPa H_2 (1000 psig) on the cesium-doped catalyst. Solid lines represent model calculations using parameter values in Table 3.

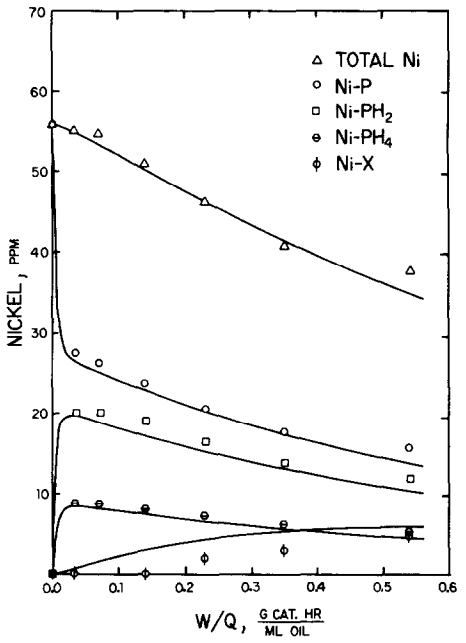

FIG. 4. Concentration versus contact time results for Ni-T3MPP at 56 ppm Ni feed, 345°C, and 6.99 MPa H_2 (1000 psig) on the sodium-doped catalyst. Solid lines represent model calculations using the parameter values in Table 3.

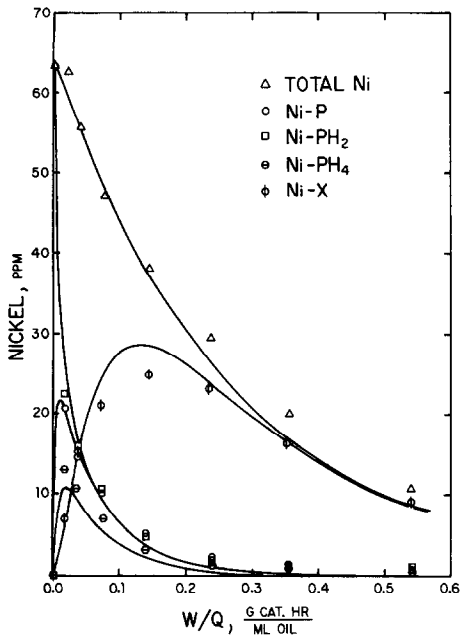

FIG. 5. Concentration versus contact time results for Ni-T3MPP at 63 ppm Ni feed, 345°C, and 6.99 MPa H_2 (1000 psig) on the oxide catalyst. Solid lines represent model calculations using the parameter values in Table 3.

X, and high ratios of k_6/k_5 which prevented buildup of Ni-X.

Slow metal removal rates were also observed, being more pronounced on the cesium sample. The resulting large discrepancy between the initial rate of Ni-P and total metal removal was an indication that metal deposition (hydrogenolysis) was the rate-limiting step in the reaction sequence.

The results on the oxide and sulfided catalysts, Figs. 5 and 6, have previously been discussed in Parts I (*4*) and II (*5*) and will be only briefly reiterated. On both catalysts, feed porphyrin was rapidly hydrogenated forming Ni-PH_2 and Ni-PH_4. The concentration of these species then declined as metal was removed from the oil and as Ni-X was generated. At the higher contact times, essentially all metal in the oil was present as this nonporphyrinic intermediate and its removal determined the total removal rate. This indicated a small ratio of k_7/k_5 to direct Ni-PH_4 toward Ni-X, and a small ratio of k_6/k_5 to accumulate Ni-X. The base-case oxide catalyst exhibited a total metal removal rate greater than that obtained on the alkali-doped samples but the rapid disappearance of Ni-P compared to total metal indicated that hydrogenolysis was still rate limiting. Sulfiding the catalyst enhanced all reaction steps relative to the oxide catalyst but not to the same extent. The metal-deposition reactions were selectively accelerated as demonstrated by the comparatively short contact time scale in Fig. 6 and were only marginally rate limiting.

The iodized catalyst (data in Fig. 7) produced lower concentrations of hydrogenated intermediates (Ni-PH_2 and Ni-PH_4) and a relatively slow rate of feed porphyrin removal compared to the oxide catalyst. There was likewise only a small contribution of Ni-X to the total pool of metal. This indicated larger ratios of k_7/k_5 and k_6/k_5. The approach of the Ni-P disappearance rate to the total metal removal rate suggests

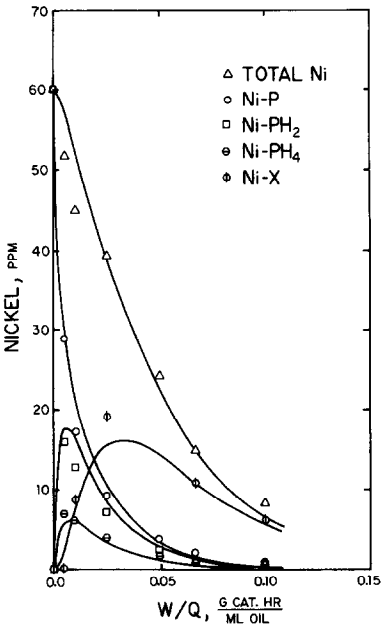

FIG. 6. Concentration versus contact time results for Ni-T3MPP at 60 ppm Ni feed, 345°C, and 6.99 MPa H_2 (1000 psig) on the sulfided catalyst. Solid lines represent model calculations using parameter values in Table 3.

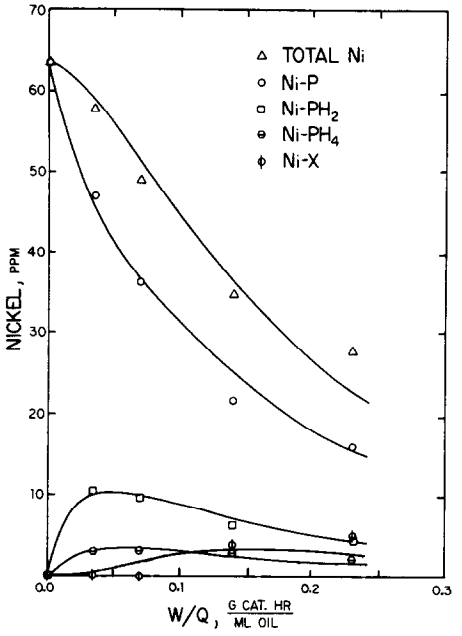

FIG. 7. Concentration versus contact time results for Ni-T3MPP at 63 ppm Ni feed, 345°C, and 6.99 MPa H_2 (1000 psig) on the iodized catalyst. Solid lines represent model calculations using the parameter values in Table 3.

that hydrogenation is now the rate-limiting step on this catalyst. A similar but more pronounced effect was seen on the chlorided catalyst in Fig. 8. Here the feed porphyrin accounted for 80% of the metal in the oil at all times compared to generally less than 20% on the oxide catalyst. The parallel feed porphyrin and total metal removal curves indicated that the initial hydrogenation step was rate limiting. The low concentration of Ni-PH_2 and the absence of Ni-PH_4 and Ni-*X* were interpreted on the basis that hydrogenated intermediates, once generated, react rapidly in relation to their production rate to deposit metal. The ability to close the Ni-T3MPP metal balance in the effluent with Ni-P and Ni-PH_2 at all contact times was unique to the chlorided catalyst.

The reactivity of Ni-T3MPP on the bare alumina support was also examined and found to be mechanistically unchanged from the $CoMo/Al_2O_3$ catalyst. All reaction steps were slower. It was difficult, however, to assess the activity of just the alumina due to the generation of a nickel-coated surface as demetallation proceeded.

Quantitative interpretation of the kinetic results on all catalysts was obtained both in terms of pseudo-first-order kinetics for total metal removal and in terms of the sequential reaction network proposed for Ni-T3MPP in Part I (*4*) and shown in Fig. 2.

It was also possible to use this network to explain the chlorided catalyst data even though Ni-PH_2 was the only stable intermediate detected. Based on the reasoning that metal removal from Ni-PH_4, in particular step k_7, is much faster than the rate of Ni-PH_4 production, k_3, the network simplifies to

$$\text{Ni-P} \underset{2}{\overset{1}{\rightleftharpoons}} \text{Ni-PH}_2 \xrightarrow{3'} \text{deposit.}$$

The similarity of this sequence to that used in Part I (*4*) to describe the behavior of

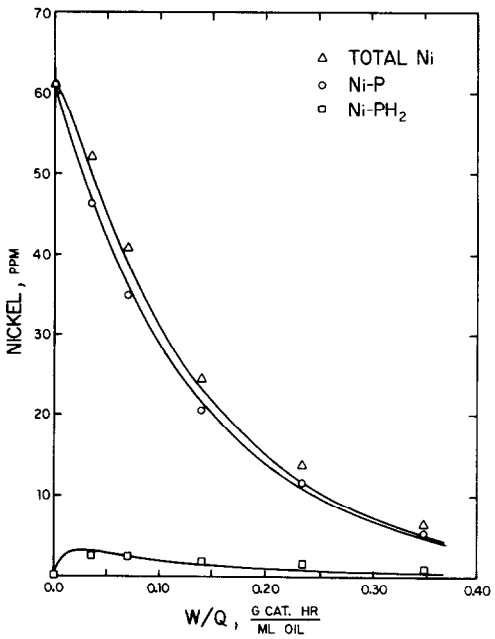

FIG. 8. Concentration versus contact time results for Ni-T3MPP at 61 ppm Ni feed, 345°C, and 6.99 MPa H_2 (1000 psig) on the chlorided catalyst. Solid lines represent model calculations using parameter values in Table 3.

TABLE 3

Kinetic Rate Parameters for Ni-T3MPP Demetallation on Modified Catalysts (345°C, 1000 psig H_2, 63 ppm Ni)

	Cs doped	Na doped	Oxide HDS-16A	Sulfided	Iodized	Chlorided	γ-Al_2O_3
k_1[a]	89.0	102.0	105.0	183.0	12.0	7.8	29.0
k_2	126.0	134.0	94.0	164.0	17.0	7.0	35.0
k_3	130.0	130.0	120.0	250.0	45.0		22.0
k_4	300.0	300.0	150.0	400.0	82.0		33.0
k_5	0	3.3	49.0	170.0	20.0		6.4
k_6	0	2.2	3.8	27.0	13.0	$k_3' = 114.0$	0.21
k_7	2.7	5.0	18.0	120.0	66.0		7.9
k_M[b]	0.33	0.75	3.4	19.3	3.8	6.4	1.0
$(k_6 + k_7)/k_1$	0.030	0.071	0.208	0.803	6.58	(14.6)	0.280
k_6/k_5	~	0.67	0.08	0.16	0.65	~	0.03
k_7/k_5	∞	1.52	0.37	0.71	3.30	~	1.23

[a] Rate coefficients are in units of ml oil/g cat. hr.
[b] First-order total metal removal.

nickel etioporphyrin (Ni-Etio) on oxide $CoMo/Al_2O_3$ is apparent. Subsequent investigation has demonstrated that the Ni-Etio behavior is not a result of chlorine contamination on the catalyst.

The kinetic parameters obtained from least-squares fitting of the experimental data to the solution (discussed in Part I (*4*)) of the coupled set of rate equations are listed in Table 3. These parameters have been used to generate the respective model curves (solid lines) in Figs. 3 through 8. The pseudo-first-order metal removal rate constants, k_M, in Table 3 were obtained from the plots of Fig. 9.

Selected rate parameters from the set in Table 3 are presented in Fig. 10. Included are the total metal removal rate constant, k_M, which although being a pseudokinetic parameter is a measure of the overall activity of the catalyst, and the porphyrin hydrogenation rate (k_1) and the hydrogenolysis, or metal-deposition rates ($k_6 + k_7$). Trends observed in these rate coefficients could be correlated with the electron affinity of the added element. This parameter is a measure of the electron attraction power of the atom (*30*). The larger (more negative) the electron affinity, the greater the attraction of an electron to an available orbital in the atom. Considering the complexity of the system under study, the apparent success of this correlation may be a fortuitous coin-

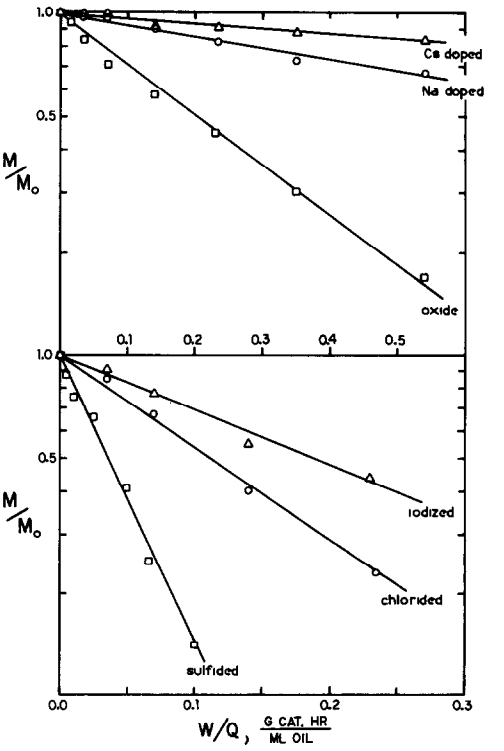

FIG. 9. First-order total metal removal plots for Ni-T3MPP at 345°C and 6.99 MPa H_2 (1000 psig) on the modified catalysts.

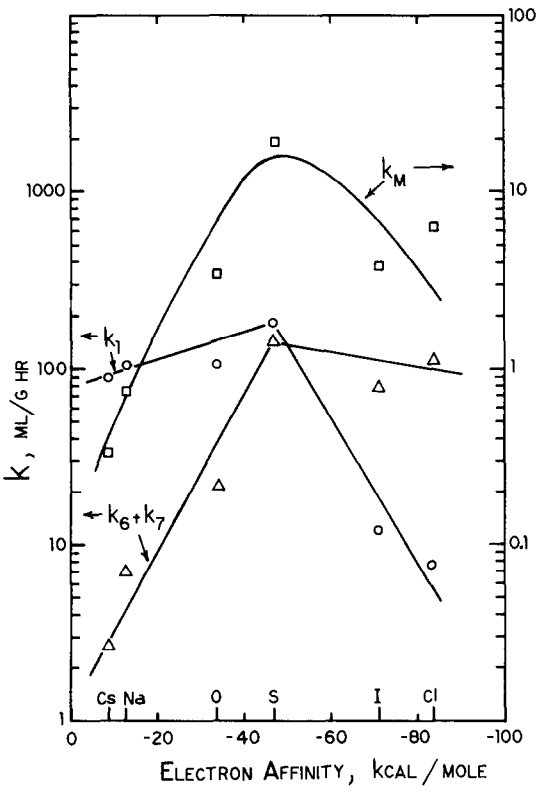

FIG. 10. Ni-T3MPP kinetic rate parameters at 60 ppm Ni feed, 345°C, and 6.99 MPa H_2 (1000 psig) versus electron affinity of dopant on the modified catalysts.

cidence and should be viewed with caution. It is tempting, however, to interpret this trend as possible evidence for a systematic modification of the surface chemistry or acidity of the catalyst in the presence of these dopants which influences the observed catalytic behavior.

Variations in catalytic activity for total metal removal as large as 50-fold were observed on the doped catalysts. When plotted in the fashion of Fig. 10, the overall demetallation rate exhibited a "volcano"-shape curve with maximum metal removal activity occurring on the sulfided catalyst. By resolving this lumped parameter into the individual reaction steps within the network, it was possible to explain why the maximum was observed. The sulfided catalyst exhibited high activity for both hydrogenation (two times greater than oxide catalyst) and metal deposition (seven times greater than oxide catalyst) resulting in the high overall demetallation rate.

On the base-case oxide catalyst and alkali-doped catalysts, the hydrogenation activity was similar. The metal-deposition rate parameters were substantially lower, hence rate limiting, and became progressively smaller moving from the oxide, to sodium-, to cesium-doped catalyst. The sharp rise in overall demetallation activity observed in progressing from the cesium-doped through to the sulfided catalyst (increasing electron affinity of additive) was attributable to this sharp increase in the rate-limiting step of metal deposition.

A quite different effect was seen when pretreating the catalyst with additives of even higher electron affinity (S, I, Cl) in a reducing environment. The lower overall demetallation activity on the iodized and chlorided catalyst was due to a significant decline in hydrogenation (k_1) activity of the catalyst which became rate limiting when progressing from sulfur to chlorine on the surface. As shown in Fig. 10, the metal-deposition activity ($k_6 + k_7$, or $k_{3'}$ for chlorided catalyst) displays only a marginal drop with increasing electron affinity of dopant whereas the hydrogenation activity is 20 times lower on the chlorided catalyst compared to the sulfided catalyst. This sharp decline in hydrogenation rate results in a shift in the rate-limiting step from hydrogenolysis on the sulfided catalyst (also on the oxide and alkali-doped catalysts) to hydrogenation on the halogen-treated catalysts.

A measure of the consistency of the kinetic parameters can be obtained by examining the relative k_1/k_2 and k_3/k_4 ratios for all catalysts. These ratios reflect the thermodynamic equilibrium between Ni-PH_2/Ni-P and Ni-PH_4/Ni-PH_2 and should therefore be invariant from one catalyst to the next. The k_1/k_2 ratio was equal to 0.91 ± 0.20 whereas k_3/k_4 was equal to 0.58 ± 0.19. Variations in these ratios were on the order of 20 to 30%.

These ratios were sensitive to the measured concentrations of Ni-P, Ni-PH_2, and Ni-PH_4 at high Ni-P conversion (>50%) where accurate measurement by uv–visible spectroscopy of the composite oil was most difficult. These variations seem reasonable in view of this limitation.

4. DISCUSSION OF ACTIVE SITES ON MODIFIED CATALYSTS

It is possible to speculate that the catalyst has two sets of sites. One set is responsible for the reversible hydrogenation reactions with rate constants k_1 and k_3, and the dehydrogenation reactions with rate constants k_2 and k_4. When the acid and base dopants were added, these four rate constants changed in a proportional manner.

The second set of sites is responsible for the irreversible hydrogenolysis reactions with rate constants k_5, k_6, k_7. These three reactions are second order with respect to hydrogen pressure, discussed in Part I (*4*). When dopants were added, the ratios of these three rate constants do not remain fixed.

Evidence obtained on these catalysts suggests that acid site density (meq/cm^2) and hydrogenolysis ($k_6 + k_7$) activity in HDM are related. This is consistent with the demonstrated correlation between acidity and activity for hydrogenolysis in HDS reactions (*31, 32*). The order of increasing acid site density, Cs < Na < γ-Al_2O_3 < CoMo, correlated with the observed increase in $k_6 + k_7$.

The superior metal-depositing activity of the oxide catalyst compared to the support indicates all hydrogenolysis activity, and acidity, is not associated with the alumina. The contribution of the Co and Mo species to the total acidity was verified by the acid density measurements here and elsewhere (*10*).

In the presence of high loadings (2 mmole/g cat.) of alkali dopants on a surface highly covered with Mo (~50% coverage for HDS-16A), the alkali is likely to interact with both the alumina and the transition metals. Therefore, the inhibition in hydrogenolysis activity associated with the alkali is likely due to a neutralization of both the alumina surface (*16*) and electron acceptor sites on Mo vacancies. The larger effect seen with Cs is consistent with its lower electron affinity.

Evidence for the existence of hydrogenation sites with acidic properties on the oxide $CoMo/Al_2O_3$ catalyst was present in Part II (*5*) with the discussion of the pyridine-poisoning results. These sites were speculated to be Mo anion vacancies on the surface. The presence of strong hydrogenation activity on the catalysts with little or no surface acidity after sodium or cesium doping suggests one of two possibilities. Once deposited, the dopants may not interfere with the *in situ* generation of additional Mo vacancies. Hence, even though these acidic sites are poisoned on the fresh oxide catalyst, under the reducing reaction conditions new sites may emerge. Alternatively, a second type of hydrogenation site may exist. This nonacidic hydrogenation site may be associated with metallic species such as cobalt which has been detected on reduced $CoMo/Al_2O_3$ catalysts (*22*) not exposed to air prior to analysis. Part of the promoting role of cobalt has been attributed to increased hydrogenation activity (*33*).

Some of this hydrogenation activity may be associated with nickel from the reacting porphyrin which deposits over the partially deactivated sites. However, the activity of the base alumina which also developed a surface covered with nickel was only one-third as active (compare k_1 values) as the alkali-doped catalysts. Thus the majority of the hydrogenation activity on these alkali-doped catalysts must be due to Co and Mo species on the surface not deactivated by the dopant.

The enhanced metal-deposition activity of the sulfided catalyst discussed in Part II (*5*) was attributed to the presence of an increased concentration of Brønsted acidity. The generation of these sites was proposed by Yang and Satterfield (*34*) to be due to

H_2S adsorbing and dissociating on Mo vacancies. A similar phenomenon may be occurring on the halogenated catalysts, with the HI and HCl generated during pretreatment also dissociating on Mo. This is especially likely when $CHCl_3$ is in the feed as HCl is then continually generated and in equilibrium with the catalyst.

Considering this adsorption and dissociation process to be responsible for the enhanced surface acidity of these catalysts, it is doubtful that a true measure of the catalyst acidity under reaction conditions can be obtained from the TPAD as performed. The acidity would obviously depend on the partial pressure of the dissociating species (H_2S, HI, HCl) and no such components are present in the gas phase during these measurements. Thus determining the absolute magnitude of the surface acidity increase on these treated catalysts over the oxide catalyst may be a difficult task. However, it is apparent from the acid density measurements that qualitatively the number of sites on these catalysts is greater than on the oxide catalyst.

The presence of chlorided alumina on the surface of the prechlorided catalyst suggested by the XPS results may also be contributing to the metal-deposition activity observed on this catalyst. The high hydrocracking activity of chlorided alumina has been reported in asphaltene and model coal liquid degradation studies (*35*). This additional bond-cleavage activity is consistent with the high rate of metal deposition which results in Ni-PH_2 as the only stable intermediate.

As demonstrated by the kinetic results in the previous section, the most significant impact due to the presence of iodine and chlorine on the catalyst was a dramatic reduction in hydrogenation activity. Treating the catalyst with these additives in a reducing environment promotes I and Cl interaction with vacancies on molybdenum, normally associated with hydrogenation activity, much like the Mo-SH groups that form in the presence of H_2S (*34*). The XPS results while not conclusive were consistent with the presence of molybdenum–halide species.

The presence of I and Cl is postulated to alter the surface electron density of the Mo by occupying active sites (generated by reduction), thereby eliminating their availability for hydrogen adsorption and double-bond coordination. Sulfur (present as SH after H_2S dissociation) also occupies these vacancies but is readily desorbed as evidenced by the high hydrogenation activity on this catalyst. Similar interpretations have been considered by Kiskinova and Goodman (*36*) when interpreting the reactivity of Ni surfaces modified with electronegative adatoms (Cl, S, P).

The stronger inhibition seen with Cl than with I is consistent with its greater electron affinity enabling it to form a more stable, more irreversibly bound molybdenum complex. Binding energies for desorption of halogens from molybdenum surfaces measured by Bolach and Blais (*37*) were progressively smaller moving down the periodic column (F > Cl > Br). Based on these binding energy strengths, less of an inhibiting effect would be expected with I than with Cl as is observed. The strength of the Mo–Cl interaction was experimentally demonstrated by the inability to restore the hydrogenation activity of a prechlorided catalyst to the activity of the oxide catalyst after exposure to flowing hydrogen at 450°C for 4 hr.

5. DISCUSSION OF REACTION ENGINEERING IMPLICATIONS

The implications of this ability to selectively alter one functionality of the catalyst and hence selectively change the relative reaction rates within the Ni-T3MPP demetallation network are revealed in the metal-deposition profiles within catalyst pellets obtained under diffusion-limited conditions. Presented in Fig. 11 are metal-deposition profiles in 1/16-in. pellets calculated with the model developed in Part I (*4*) using

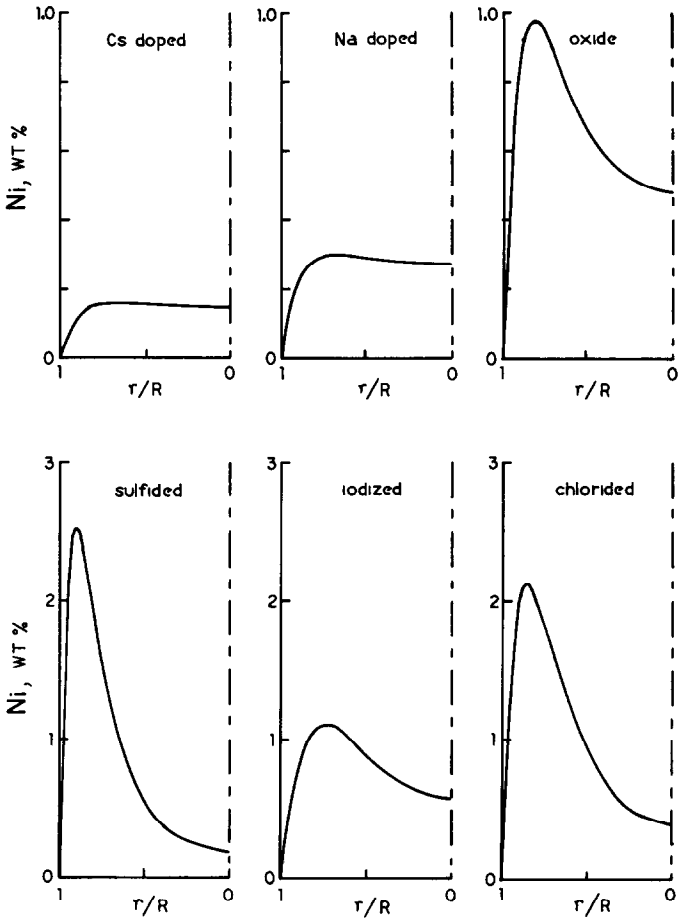

FIG. 11. Calculated nickel-deposition profiles in 1/16-in.-diameter catalyst pellets at the reactor entrance for Ni-T3MPP demetallation at 345°C and 6.99 MPa H_2 (1000 psig) on the modified catalysts.

the kinetic parameters presented in this paper for the different catalysts. The profile for the chlorided catalyst was calculated using the model for Ni-Etio developed by Agrawal (*29*), as the kinetic reaction schemes were analogous. These profiles are calculated for the entrance of the bed ($z = 0$). The oxide and sulfided catalyst profiles have been experimentally verified and discussed in Parts I (*4*) and II (*5*). All nonkinetic parameters used in calculating the other plots (Cs, Na, I, and Cl doped) were identical to those used for the oxide catalyst listed in Part I (*4*).

The Thiele moduli, ϕ_i for the uncoupled system of pseudocomponents reacting by first-order irreversible kinetics in the solution technique given by Wei (*38*) characterize the extent to which diffusional limitations are important in the metal profiles. Listed in Table 4 are the Thiele moduli for each set of kinetic data calculated from the eigenvalues of the diffusion coefficient and rate coefficient matrices discussed in Part I (*4*). These parameters are the characteristic decay rates of concentration versus radial distance in the terms summed to obtain the metal profiles:

$$M(r,z) = \sum_i b_i(z) \frac{I_0(\phi_i r/R)}{I_0(\phi_i)},$$

where $M(r,z)$ is the concentration of depos-

TABLE 4

Characteristic Thiele Moduli and Metal Distribution Parameters for Modified Catalysts
Ni-T3MPP (345°C, 6.99 MPa H_2 (1000 psig))

$$M = \sum_i b_i(z) \frac{I_0(\phi_i r/R)}{I_0(\phi_i)}$$

	$b_1(0)^a$	ϕ_1	$b_2(0)$	ϕ_2	$b_3(0)$	ϕ_3	$b_4(0)$	ϕ_4	θ_m
Cs	1.00	0.805	−1.48	16.41	−0.93	24.71	0	0	0.93
Na	1.00	1.42	−0.74	1.62	−0.49	17.20	0.23	25.10	0.92
Oxide	1.00	2.13	0.56	4.81	−3.23	15.98	1.65	22.08	0.66
Sulfide	1.00	4.29	1.91	8.43	−4.26	23.90	2.10	33.38	0.36
Iodize	1.00	3.43	−0.62	3.94	−0.50	7.58	0.11	15.31	0.75
Chloride	1.00	4.17	−1.00	12.07					0.50

[a] All b_i are normalized to b_1.

ited metal at a given radial, r, and axial, z, position. The relative magnitude of the coefficients, b_i, also listed in Table 4, indicates all terms contribute to the shape of the profiles. The large ϕ_i terms decay rapidly from maxima at $r/R = 1.0$, leaving the slower decaying components to dominate the region of small r/R.

Consistent with the slower metal deposition steps ($k_6 + k_7$) on the Cs- and Na-doped catalysts, the smallest Thiele moduli have values near one or lower, and, correspondingly, uniform metal profiles are seen on these catalysts. The continuous increase in the smallest ϕ_i on progressing from the Cs-doped to the sulfided catalyst reflects an increasingly stronger diffusion limitation in the deposition reactions as is revealed in the metal profiles.

It is possible to compare the deposition patterns of metal in the catalyst extrudates quantitatively using the metal distribution parameter defined by Tamm *et al.* (*1*):

$$\theta_m = \frac{\int_0^1 M(r) r\, dr}{M_{max} \int_0^1 r\, dr},$$

where $M(r)$ is the local weight percentage metal deposit, M_{max} the maximum concentration, and r the fractional radius. This parameter is essentially the ratio of the average metal concentration to the concentration at the maximum and characterizes the effective utilization of the catalyst for metal deposits. A distribution parameter of unity corresponds to uniform metal profiles whereas a value approaching zero would be characteristic of a sharp spike at the pellet's edge. Values calculated at the entrance of the bed for each catalyst are listed in Table 4.

Catalysts (Cs and Na doped) with small ϕ_i (slow deposition rates) were calculated to have high distribution parameters. As metal-deposition activity increased (large ϕ_i), θ_m decreased and less effective use was made of the metal-loading capacity of the catalyst. Catalysts with small θ_m reach the plugging limit at M_{max} more quickly and with less total metal in the catalyst (i.e., $\theta_m \times M_{max}$) than is typical for more uniform distributions. The highly desirable uniform profiles are obtained at the expense of somewhat lower total metal conversion at equivalent contact times. Hence the optimum conditions for metal deposition would be a balance between high conversion and most complete utilization of the catalyst.

CONCLUSIONS

The results of this doping study have shown how selective alteration of the relative hydrogenation/hydrogenolysis (metal

deposition) rates in the HDM network of Ni-T3MPP are possible, enabling dramatic shifts in the overall rate-limiting step. This suggests that the reactivity of metal compounds in residuum oils may be manipulated to control the location where metals deposit within catalyst pellets during hydroprocessing.

A relationship between hydrogenolysis (metal deposition) activity and surface acidity has been demonstrated. Addition of Cs and Na to the $CoMo/Al_2O_3$ catalyst lowered the acidity and selectively reduced the metal-deposition steps ($k_6 + k_7$) without inhibiting hydrogenation (k_1).

The overall impact of I or Cl treatment on the activity of the CoMo catalyst can be interpreted in terms of two effects resulting from the interaction of HI or HCl with vacancies on the molybdenum. The dissociation of these species on Mo sites generated by reduction produces Brønsted acidity which maintains a high level of hydrogenolysis activity ($k_6 + k_7$) promoting metal deposition. The simultaneously generated molybdenum–halide bond eliminates a site otherwise available for hydrogenation, lowering the total number present and the observed activity (k_1).

Sulfiding had the unique effect of producing an enhancement in both the hydrogenation and hydrogenolysis activities over the oxide catalyst. The increase in hydrogenolysis ($k_6 + k_7$) activity was selectively larger and was consistent with an increase in Brønsted acidity arising from H_2S dissociation on Mo vacancy sites.

Catalyst selectivity for Ni-*X* formation requires low ratios for both k_6/k_5 and k_7/k_5 and was diminished in the presence of all dopants. Only on the sulfided catalyst did the dominance of this species in the oil at high feed conversions approach that observed with the oxide catalyst. The slow demetallation rate (k_6) of this nonporphyrinic compound suggests that high selectivity for Ni-*X* is desirable from a standpoint of obtaining uniform metal deposits in catalyst pellets.

Calculated metal-deposition profiles in 1/16-in. catalyst pellets reflected the selectivity variations in the Ni-T3MPP reaction network caused by each dopant. Reaction in the presence of basic additives (Cs, Na) was characterized by small Thiele moduli and uniform profiles. In contrast, the acidic components (S, I, Cl) resulted in large Thiele moduli and more sharp, U-shape profiles indicative of strongly diffusion-limited deposition reactions.

ACKNOWLEDGMENTS

The authors are grateful to David Green and Chi-Wen Hung of Chevron Research Company for their helpful discussions, to Chi-Wen Hung for providing the BET surface area measurements, to Rene LaPierre and Paul Brigandi of Mobil Research and Development Corporation for providing the ammonia desorption characterization, and to John Martin of the Surface Analysis Central Facility at M.I.T. for the XPS results. The financial support of the National Science Foundation, Grant CPE 80-20852, and Chevron Research Company is also gratefully acknowledged.

REFERENCES

1. Tamm, P. W., Harnsberger, H. F., and Bridge, A. G., *Ind. Eng. Chem. Process Des. Dev.* **20,** 262 (1981).
2. Riley, K. L., *ACS Prepr. Div. Pet. Chem.* **23,** 1104 (1978).
3. Plumail, J. C., Jacquin, Y., Martino, G., and Toulhoat, H., *ACS Prepr. Div. Pet. Chem.* **28**(3), 562 (1983).
4. Ware, R. A., and Wei, J., *J. Catal.* **93,** 100 (1985).
5. Ware, R. A., and Wei, J., *J. Catal.* **93,** 122 (1985).
6. Broderick, D. H., and Gates, B. C., *AIChE J.* **27,** 663 (1981).
7. Satterfield, C. N., and Gultekin, S., *Ind. Eng. Chem. Process Des. Dev.* **20,** 62 (1981).
8. Muralidhar, G., Massoth, F. E., and Shabtai, J., *J. Catal.* **85,** 44 (1984).
9. Boorman, P. M., Kriz, J. F., Brown, J. R., and Ternan, M., *in* "Proceedings, Climax Fourth International Conference on the Chemistry and Uses of Molybdenum" (H. F. Barry and P. C. H. Mitchell, Eds.), p. 182. Climax Molybdenum Co., Ann Arbor, Mich., 1982.
10. Ratnasamy, P., Sharma, D. K., and Sharma, L. D., *J. Phys. Chem.* **78,** 2069 (1974).
11. Ramaswamy, A. V., Sivasanker, S., and Ratnasamy, P., *J. Catal.* **42,** 107 (1976).
12. Stanulonis, J. J., and Pederson, L. A., *ACS Prepr. Div. Pet. Chem.* **25,** 255 (1980).

13. Fitz, C. W., Jr., and Rase, H. F., *Ind. Eng. Chem. Prod. Res. Dev.* **22,** 40 (1983).
14. Lycourghiotis, A., Defosse, C., Delannany, F., Lemaitre, J., and Delmon, B., *J. Chem. Soc. Faraday Trans. 1* **76,** 1677 (1980).
15. Lycourghiotis, A., Defosse, C., Delannany, F., and Delmon, B., *J. Chem. Soc. Faraday Trans. 1* **76,** 2052 (1980).
16. Kordulis, C., Voliotio, S., and Lycourghiotis, A., *J. Less-Common Met.* **84,** 187 (1982).
17. Lycourghiotis, A., Defosse, C., and Delmon, B., *Bull. Soc. Chim. Belg.* **91,** 613 (1982).
18. Lycourghiotis, A., Vattis, D., Karaiskakis, G., and Katsanos, N., *J. Less-Common Met.* **86,** 137 (1982).
19. Martinez, N. P., and Mitchell, P. C. H., *in* "Proceedings, Climax Third International Congress on the Chemistry and Uses of Molybdenum" (H. F. Barry and P. C. H. Mitchell, Eds.), p. 105. Climax Molybdenum Co., Ann Arbor, Mich., 1980.
20. Bhinde, M. V., "Quinoline Hydrodenitrogenation Kinetics and Reaction Inhibition," Ph.D. thesis. University of Delaware, June 1979.
21. deBeer, V. H. J., Bevelander, C., van Sint Fiet, T. H. M., Werter, P. G. A. J., and Amberg, C. H., *J. Catal.* **43,** 68 (1976).
22. Chin, R. L., and Hercules, D. M., *J. Phys. Chem.* **86,** 3079 (1982).
23. Zingg, D. S., Makovsky, L. E., Tischer, R. E., Brown, F. R., and Hercules, D. M., *J. Phys. Chem.* **84,** 2898 (1980).
24. Walton, R. A., *J. Less-Common Met.* **54,** 71 (1977).
25. Gajardo, P., Grange, P., and Delmon, B., *J. Catal.* **63,** 201 (1980); **66,** 469 (1980).
26. Frost, D. C., McDowell, C. A., and Woolsey, I. S., *Mol. Phys.* **27,** 1473 (1974).
27. Brinen, J. S., and Armstrong, W. D., *J. Catal.* **54,** 57 (1978).
28. Ware, R. A., "Reactivity of Nickel Porphyrins in Catalytic Hydrodemetallation," Sc.D. thesis. M.I.T. September 1983.
29. Agrawal, R., and Wei, J., *Ind. Eng. Chem. Process Des. Dev.* **23,** 505, 515 (1984).
30. MacKay, K. M., and MacKay, R. A., "Introduction to Modern Inorganic Chemistry." Intern. Textbook Co., London, 1973.
31. Laine, J., Brito, J., and Yunes, S., *in* "Proceedings, Climax Third International Conference on the Chemistry and Uses of Molybdenum" (H. F. Barry and P. C. H. Mitchell, Eds.), p. 111. Climax Molybdenum Co., Ann Arbor, Mich., 1980.
32. Maternova, J., *Appl. Catal.* **6,** 61 (1983).
33. Massoth, F. E., "Advances in Catalysis," Vol. 27, p. 265. Academic Press, New York, 1978.
34. Yang, S. H., and Satterfield, C. N., *J. Catal.* **81,** 168 (1983).
35. Salim, S. S., and Bell, A. T., *Fuel* **61,** 745 (1982).
36. Kiskinova, M., and Goodman, D. W., *Surf. Sci.* **108,** 64 (1981).
37. Bolach, G., and Blais, J. C., *Surf. Sci.* **126,** 405 (1983).
38. Wei, J., *J. Catal.* **1,** 526, 538 (1962).